Landslides (2012) 9:179–187
DOI 10.1007/s10346-011-0294-4
Received: 8 April 2010
Accepted: 24 August 2011
Published online: 10 September 2011

Louis Bugnion · Brian W. McArdell · Perry Bartelt · Corinna Wendeler

Measurements of hillslope debris flow impact pressure on obstacles

Abstract We present measurements of hillslope debris flow impact pressures on small obstacles. Two impact sensors have been installed in a real-scale experimental site where 50m^3 of water-saturated soil material are released from rest. Impact velocities vary between 2 and 13m/s; flow heights between 0.3 and 1.0m. The maximum impact pressures measured over 15 events represent between 2 and 50 times the equivalent static pressures. The measurements reveal that quadratic velocity-dependent formulas can be used to estimate impact pressures. Impact coefficients C are constant from front to tail and range between $0.4<C<0.8$ according to the individual events. The pressure fluctuations to depend on the sensor size and are between 20% and 60% of the mean pressure values. Our results suggest that hazard guidelines for hillslope debris flows should be based on quadratic velocity-dependent formulas.

Keywords Hillslope debris flow · Field scale tests · Impact pressure · Impact coefficient

Introduction

A long-standing problem in the study of landslides is to quantitatively understand the pressures they can exert on obstacles as a function of impact speed, flow height and debris mixture properties. Simple and reliable formulae are required in mitigation studies to delimit hazard zones and strengthen buildings or dimension structures such as masts and pylons in debris flow torrents and runout zones or where hillslope debris flows (or open-slope debris flows) are expected. Ring-net barriers (Wendeler 2008), a new method of debris flow mitigation, also require estimates of impact pressure to adequately dimension structural elements and anchors. Pressure formulae are also helpful to analyse damage—both on man-made structures (Egli 2005) and trees (Stoffel and Bollschweiler 2009)—in historical case studies and therefore can be used to establish magnitude–frequency relations for landslide or debris flow activity in a particular region. The problem is especially relevant because new simulation tools are available that can predict flow speed and height in three-dimensional terrain (e.g., Christen et al. 2010; McDougall and Hungr 2004). Without accurate estimates of the corresponding pressures, the potential of these new tools cannot be fully realized.

Impact pressures generated by geophysical flows are complicated because they depend both on the flow mixture (which contains mud, rocks and large boulders and sometimes woody debris and air) that varies from point to point in the surge (Iverson et al. 2010) and with time and on the geometry and size of the flow as well as of the obstacle. Because of the material inhomogeneity, impact forces can fluctuate strongly over time. The rheology of the mixture is important because it influences the ability of the flow to redistribute stresses in the region of the obstacle. The presence of a solid phase can increase local impact pressure due to hard contact and material locking, a phenomenon that is observed in dry granular flows (Levy and Sayed 2008) and at the head of some debris flows.

In this report, we present measurements of flow height, front and surface velocity and impact pressure of field-scale hillslope debris flows (following the terminology of Hutchinson 1988 to refer to unchannelized debris flows on a hillslope). The volume of the material involved is 50 m^3, the maximum flow height at the location of the obstacles (30 m downstream) ranges between 0.3 and 1.0 m and the front speed at the location of the obstacles ranges between 2 and 13 m/s. These observations are made in a wide trapezoidal channel excavated into a hillslope (Fig. 1). The hillslope debris flows we generate are roughly equivalent to small debris flows on weakly channelized surfaces. Examples are described by Imura and Shimojo (2007) in Japan (Table 1) and Rickli and Bücher (2005) in Switzerland (Table 2). These field studies typically involve post-failure documentation of the initial landslide failure zone as well as the runout distance for natural events—unfortunately, data on flow velocity and impact pressure are rarely available. In some cases, rough estimates of flow properties are available (e.g., Egli and Vanomsen 2005). The flows described herein are roughly equivalent to the median volume, flow height and slope angle value of Tables 1 and 2.

Our results indicate that impact pressures on large submerged obstacles (flow heights of same order as the obstacles) scale with the square of the flow velocity. This dependency is interpreted in terms of the fraction of material that is stopped during the impact process. Although not described herein, the overall objective of this work was to investigate the performance of flexible barriers against hillslope debris flows and small shallow landslides, so considerable effort, involving evaluations by Swiss landslide experts (including practitioners), was made to produce realistic flows with a realistic sediment mixture and flow behaviour.

Methods

A 41-m-long, 8-m-wide channel is constructed on the side of a rock quarry near Veltheim, Canton Aargau, Switzerland (Fig. 1a). Sediment deposits on the hillslope are excavated down to the bedrock surface, which is a natural bedding plane parallel to the land surface, with an average slope inclination of 30°. The channel sidewalls are 1 m high and consist of soil material (which is generally not entrained by the flows). At the upper channel end, a wall is constructed out of wood beams and steel columns to create a sloping reservoir (Fig. 1b) with a maximum capacity of 50 m^3 of debris (approximately 100 metric tons). The retaining wall is 1.8 m high; the lower 0.8 m operates as a trap door, hinged at the base, that is held closed by cables. The cables are released to spill the debris material down the slope. Because the reservoir is located near a road, it can be filled by trucks which transport the material from the mixing place. The material is obtained by mixing soil and bedrock material from the quarry with water. Systematic and reproducible variation of the flow mixture composition and water

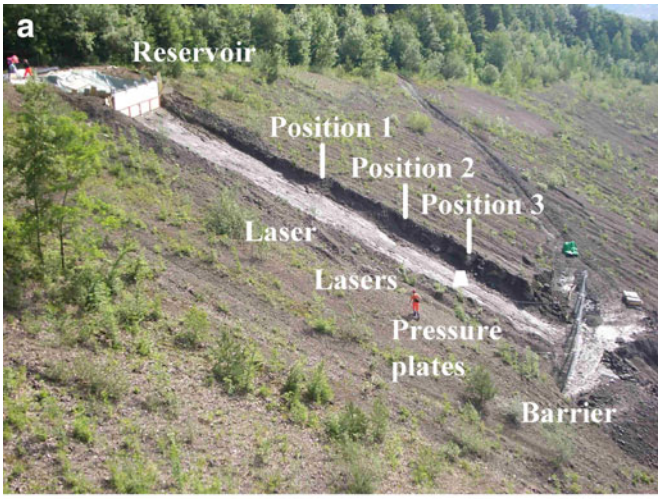

Fig. 1 Channel excavated down to bedrock in the hillslope of a disused quarry face (**a**) and material reservoir comprising the release zone (**b**). Note that the downstream end of the channel ends at a flexible barrier, which artificially limited the runout of the flows

content is not possible. On one hand, the composition of the raw materials from the quarry (bedrock and soil material) is expected to vary over large volumes and from one test to another. On the other hand, water loss during transport is inevitable and difficult to quantify. For these reasons, the proportion of the raw materials varies from one test to another and samples of material (see below) are taken from the reservoir to assess mixture composition and water content. The filling of the reservoir and the release take place within 2 h to minimize settling and consolidation. Plastic sheets are placed at the bottom of the reservoir to prevent water loss and to ensure evacuation of all material. At the lower end of the channel, a flexible steel mesh barrier stops the flow.

Upon release the material accelerates rapidly out of the reservoir and flows down the slope. Deposition on the slope begins immediately—fast flows deposit little material and accelerate over the entire channel length while slower flows deposit more material and decelerate along the second half of the channel (see Fig. 2). The volume stopped by the flexible barrier at the

Table 1 Summary of 669 events dated between 2001 and 2005 in Japan from Imura and Shimojo (2007)

	Min.	Max.	Median
Slope (°)	15	80	44
Failure depth (m)	0.2	5	1.2
Volume (m^3)	25	500	66

Slope refers to the slope angle in the failure zone

Table 2 Summary of 133 events from year 2002 in Switzerland from Rickli and Bücher (2005)

	Min.	Max.	Median
Slope (°)	23	50	34
Failure depth (m)	0.2	1.5	0.8
Volume (m^3)	30	1,100	72
Runout distance (m)	4.5	71	16.5

Fig. 2 Lateral view of release 15.1 just after release (**a**) and at the time of impact on the pressure plates (**b**)

lower end of the channel ranges between 15 and 40 m³. Vertical (slope-normal) accelerations are visible in the vicinity of the trap door, but observations of the flow surface from video recordings indicate that these rapidly disappear after several meters, leading to flows in which the primary velocity component is parallel to the slope. Video observations of the front reveal that the flow velocities across the channel width are quite constant at least until position 2; material at the slope sidewalls lags slightly behind, indicating some sidewall friction. After position 2 a small secondary surge often develops on the right side of the channel. In places, micro gullies are present on the bedrock surface, principally on the sides and in the lower part of the channel. Minor amounts of material transported by runoff due to rainfall between the tests lie on the bed surface and can be entrained by the flow. At the end of a test day, the channel is cleared out with a pressurized water hose. On tests with successive releases (between 2 and 4), deposited material (between 5 and 30 m³) from the first releases is still present on the channel bed during the consecutive releases.

The channel is instrumented with vertically oriented laser distance sensors located 14 m (position 1) and 26 m (position 2) downstream from the starting reservoir (distances measured parallel to the slope). The sensors hang from cables and are used to determine the flow heights at the middle of the channel. The flow heights reported here correspond to the height perpendicular to the bed surface. At position 2, two laser distance sensors are spaced 30 cm with their beams parallel and directed at the flow surface. The velocity of the upper flow surface is derived using the discrete cross correlation function $h_1h_2(t, \Delta t)$ of the two height signals

$$h_1h_2(t,\Delta t) = \sum_{t'=t-\text{bin\_size}}^{t+\text{bin\_size}} \frac{h_1(t') - E_{h_1}}{\sigma_{h_1}} \frac{h_2(t'+\Delta t) - E_{h_2}}{\sigma_{h_2}} \quad (1)$$

where $h_1(t)$ and $h_2(t)$ are the two flow height time series. The bin_size parameter is the time interval over which the cross correlation function is calculated. It was set to 0.125 or 0.25 s. E_{h_1} and E_{h_2} are the mean values of the flow heights over the bin_size while σ_{h_1} and σ_{h_2} are the standard deviations of the flow heights over the bin_size.

Four metres downstream of position 2 at 30 m downslope (position 3), two pressure plates are mounted on cube-shaped wedges to measure impact forces (see Fig. 3). The smaller wedge has dimensions 160 mm (width) × 225 mm (height); the larger wedge 240 mm (width) and 295 mm (height). The heights of the wedges are measured from the concrete plate that is flush with the channel bed. Thus, both wedges are completely submerged when the flow heights are greater than 295 mm, which is the case most of the time (see Table 3 and Fig. 5). Cylindrical strain-gauge sensors with diameter 120 mm and measuring range up to 20 kN are built in to the wedges. They are each surmounted by two square steel plates with side lengths 120 and 200 mm (A=0.0144 and 0.04 m²), respectively. The steel plates are separated by an elastomer layer of 20 mm thickness for overload protection (SBR elastomer with hardness 65 shore A). The screws holding the steel plates and the elastomer layer together only press on the outer plate so that the impulses are damped by the elastomer layer. The centres of the steel plates are located 0.14 m and 0.17 m above the ground, and the two sensors are separated laterally by 1 m. Between tests 11.2 and 13.1, the locations of the large and small pressure plates were exchanged.

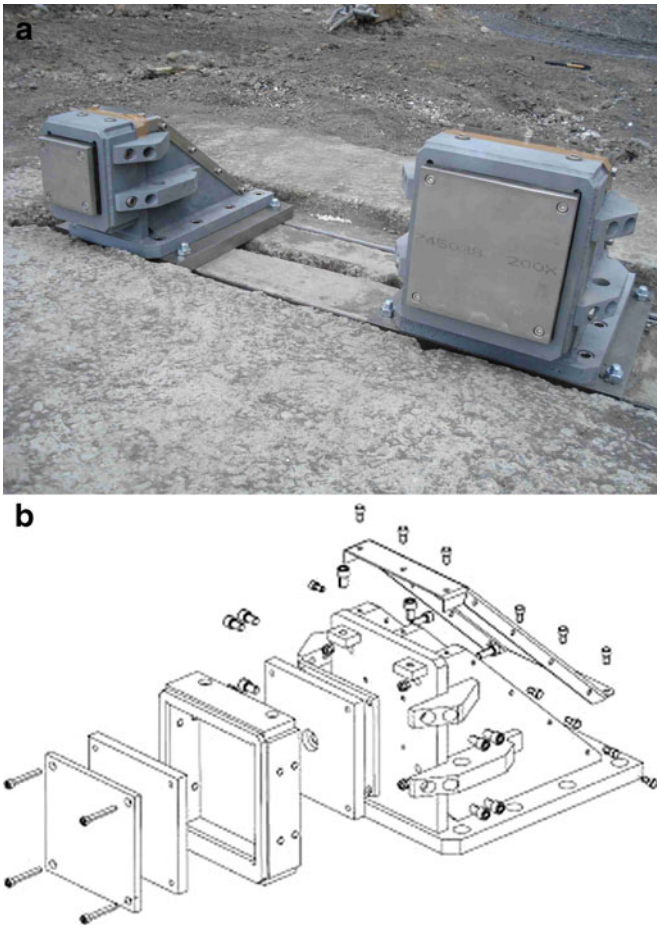

Fig. 3 **a** Small and large wedges and **b** the design drawing of the large wedge. The pressure sensors are located on the upslope-oriented face of the wedges

The strain-gauge sensors deliver a 2-kHz signal. They are filtered to remove oscillations due to hard contacts between solid grains and the pressure plates. The filtering consists of replacing each signal value by the mean value over 0.05-s time intervals. The choice of the time interval is based on calibration tests of the pressure plates and corresponds to the duration of the pressure oscillation consecutive to a hard contact. A steel sphere (mass=190 g) attached to a string (see Fig. 4) is released from different heights on the pressure plate (impact velocities between 0.5 and 1 m/s, rebound velocities between 0.1 and 0.3 m/s). Because the pressure plate is not perfectly rigid (due to the elastomer layer), it vibrates under the effect of the hard contact and the recorded pressure oscillates around zero (see Fig. 4b). The duration of the oscillation is of the order of 0.02 to 0.03 s. The mean pressure value taken over the duration of the oscillation scales with the momentum exchanged between the steel ball and the pressure plate while the median value taken over the duration of the oscillation is close to zero. The filtering of the pressure signal does not modify the integral of the pressure signal over time that is equal to the momentum exchanged between the flow

Table 3 Summary of Veltheim tests

Release no.	Mean front velocity (m/s)	Max. flow height at position 2 (m)	Wet density (kg/m^3)	Water mass fraction (%)	Fines mass fraction (%)	Gravel mass fraction (%)	Liquid limit (%)	Plastic limit (%)	Plasticity index (%)
4	5.3	0.59	1,850	22	46	28	30	17	13
5	8.4	0.41	1,920	21	36	40	28	17	11
6	10.3	0.51	1,950	24	21	59	27	15	12
7.1	9.5	0.32	1,760	20	34	33	29	16	13
7.2	10.4	0.66	–	–	–	–	–	–	–
8.1	8.0	0.38	1,840	25	38	35	32	15	17
8.2	9.2	0.79	1,880	23	31	44	31	15	16
9.1	10.2	0.29	1,790	28	48	16	27	13	14
9.2	9.6	0.9	–	–	–	–	–	–	–
9.3	9.9	0.6	–	–	–	–	–	–	–
10	8.2	0.4	1,900	18	21	46	24	15	9
11.1	9	0.38	2,060	16	27	48	33	17	16
11.2	9.4	0.42	–	–	–	–	–	–	–
13.1	8.4	0.33	1,880	22	28	37	26	17	9
13.2	9.1	0.54	–	–	–	–	–	–	–
14.1	9.1	0.4	1,990	17	25	48	31	18	13
14.2	9.6	0.88	2,030	14	–	–	–	–	–
14.3	9.1	0.8	1,930	19	–	–	–	–	–
14.4	8.6	0.8	–	–	–	–	–	–	–
15.1	8.9	0.37	1,830	23	25	41	29	16	13
15.2	9.1	0.99	–	–	–	–	–	–	–
16.1	6.4	0.37	2,110	14	41	26	33	17	16
16.2	9.1	0.74	–	–	–	–	–	–	–

On tests 1 to 3 and 12, the pressure plates are not installed or are defective

The mean front velocity is the mean front velocity calculated between position 1 and position 2. "Fines" refer to both clay and silt content ($d < 0.063$ mm). The liquid and plastic limits are the consistency limits for the fines content and the plasticity index is the difference between the liquid and plastic limits

and the plate. The pressure oscillations that are characteristic of the pressure plate vibrations are replaced by mean pressure values that are related to the solid grain properties. The mean values, median values and standard deviation of the pressure signals are computed over the same 0.05-s time intervals. Only small deviations are noticed between the signals filtered with the mean or with the median value indicating that the contribution of hard contacts to the pressure signals are short and punctual. The deviations coincide with peaks in the standard deviation time series.

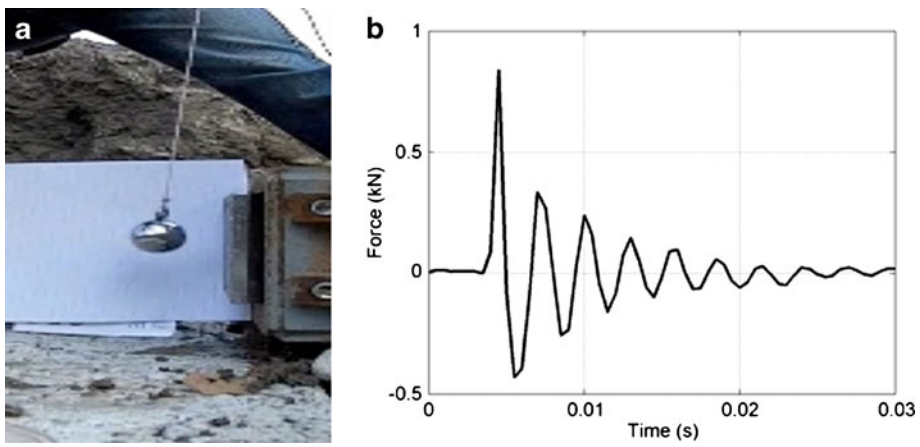

Fig. 4 **a** Setup for calibration tests of the pressure plates. **b** Force oscillation measured during one hard contact between the steel ball and the small pressure plate

Results

Between September 2008 and September 2010, we have performed 16 tests (see Table 3). Most tests consist of one single release of 50 m^3 debris material. On tests 7, 8, 11, 13, 15 and 16, two successive releases are carried out while on test 9 three releases and on test 14 four releases take place successively (the volume released is always 50 m^3). Between consecutive releases (between 2 and 3 h) deposited material remains on the channel bed surface. Material samples are collected from the top of the reservoir before every first release (and before second release 8.2 and in the deposit after release 7.1) and are analysed in the laboratory for density, water content, grain-size distribution and consistency limits of the fines content (see Table 3 and Fig. 5). The volume of the samples (about 30 kg) is large enough to assess the grain-size distribution accurately for grain sizes up to 60 mm. For grain sizes up to 100 mm samples of 250 kg would be necessary (in order to have a volume of the sample hundred times larger than the volume of the grain). The mass fraction of cobbles larger than 60 mm (ranging between 0% and 5%) is thus removed from the results and the other mass fractions are adjusted accordingly. On release 7.1, two material samples are collected; one in the reservoir and one in the deposit at the flexible barrier. The properties of the two samples are very close (maximum deviation of 8% for the clay mass fraction), indicating that the sample taken at the surface of the reservoir is representative for the whole material contained in the reservoir.

The density of the debris mixtures ranged between 1,760 and 2,110 kg/m^3 and the water content between 14% and 28% (percentage of mass). The mass fraction of fines (grain size $d < 0.063$ mm) and gravel (2 mm $< d <$ 60 mm) vary between 21% and 48% and 16% and 59%, respectively. The mean front velocity calculated between position 1 and 2 varies between 5.3 and 10.4 m/s, and the maximal flow heights at position 2 range between 0.29 and 0.99 m. The maximum impact pressure ranges between 15 and 200 kPa (see Table 4). The passing time of the front is defined as the time when the height is equal to 0.05 m. From the pressure signals, it is defined when the pressure reaches 10 kPa.

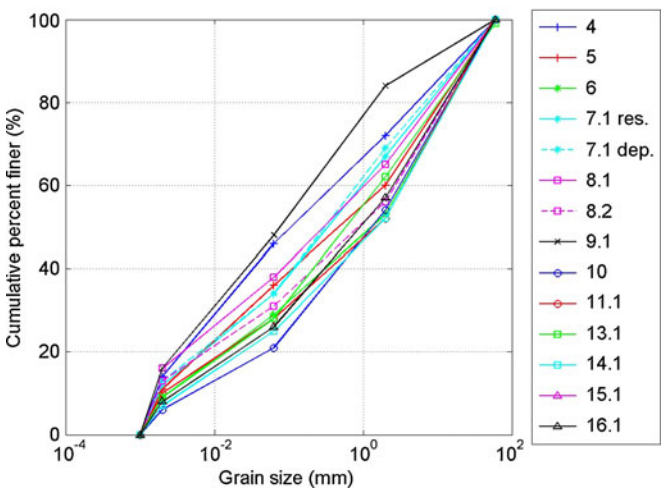

Fig. 5 Grain-size distributions for releases 4 to 16.2, the data points represent the silt, clay, sand and gravel mass fraction. For release 7.1, the grain-size distributions of samples from the reservoir and the deposit are plotted

Flow height

Two main types of flow front can be recognized. Flows on the slope free of sediment deposits have a moderately steep front followed by a body with smoothly varying flow height. The maximum flow heights range between 0.3 and 0.5 m and are measured between 0.5 and 1.5 s after the passing of the front. Flows on the slope with previously deposited material show steeper fronts and a shorter body. The maximum flow depths range between 0.6 and 1 m and are measured between 0 and 0.5 s after the passing of the flow front. The peak heights correspond to the aerated (and unsaturated) upper part of the front region of the flow. A prominent feature of all the flows is the presence of a tail, indicated by decreasing flow heights with time. A constant surface elevation at the end of the measurement indicates that the material has stopped moving. The deposition heights at positions 1 and 2 range between 0.03 and 0.28 m. The deposition heights correlate negatively with the mean front velocity from Table 3. The mean of deposition heights at positions 1 and 2 after first releases are considered (because the deposition heights after consecutive releases are affected by the deposition heights from the preceding releases) (Fig. 6).

Front and surface velocities

Mean front velocities between positions 1 and 2 are computed from the front passing times at the laser sensors (see Table 3). They range between 5.3 and 10.4 m/s. For the analysis of the impact pressure data, the front velocities between positions 2 and 3 are determined from the front passing times at the laser sensor and from the impact times on the pressure plates (see Table 4). This results in different front velocities at the locations of the large and small pressure plates due to different impact times. Surface velocities at position 2 are presented in Fig. 7 for releases 14.1 to 14.2.

Comparing first releases (on the bedrock flow surface without sediment deposits from subsequent releases), we can distinguish a difference in flow behaviour among releases with a large fraction of coarse particles (gravel fraction between 45% and 50%, releases 6, 10, 11.1, 14.1 and 15.1). They all are fast flows independently of water content or liquidity index. The liquidity index LI is defined on the base of the plastic limit PL and the liquid limit LL of the fines content and situates the water content W in connection to the consistency limits PL and LL:

$$\mathrm{LI} = \frac{W - \mathrm{PL}}{\mathrm{LL} - \mathrm{PL}} \qquad (2)$$

A second category includes releases with large fines content, i.e., clay and silt fraction larger than 40% (releases 4, 9 and 16). The front velocities of these releases are lower on average and display scatter but correlate with the liquidity index.

Impact pressure

The maximum impact pressures range between 15 and 200 kPa, i.e., over 1 order of magnitude. Alternatively, the impact pressures are 2 to 50 times larger than the static pressure values. In Fig. 8, the raw and filtered time series of the impact pressure signals measured during release 15.1 by the large pressure plate are plotted. The maximum impact pressures are measured in the front of the flow

Table 4 Maximum impact pressure on large and small plates and impact coefficient values for releases 4 to 16.2

Release no.	Front velocity (m/s) on		Max. pressure (kPa) on		Impact coeff. C () on	
	Large plate	Small plate	Large plate	Small plate	Large plate	Small plate
4	2.2	2.3	17.2	18.4	2.00	1.87
5	6.8	8.6	61.5	92.9	0.69	0.65
6	–	10.8	–	106.1	–	0.47
7.1	–	8.6	–	112.5	–	0.86
7.2	–	6.1	–	75.2	–	1.17
8.1	7.2	9.3	41.7	72.9	0.44	0.46
8.2	6.5	8.1	28.1	86.2	0.36	0.69
9.1	8.3	9.3	65.9	135.6	0.53	0.87
9.2	5.2	5.5	48.7	96.3	0.99	1.79
9.3	5.7	8.3	44.6	146.3	0.77	1.20
10	9.0	8.9	96	201.1	0.62	1.34
11.1	7.9	–	94.6	–	0.74	–
11.2	8.9	–	83	–	0.51	–
13.1	9.5	8.9	98.5	138.8	0.58	0.93
13.2	10.5	–	123.7	–	0.60	–
14.1	9.4	–	138	–	0.79	–
14.2	9.3	–	132.5	–	0.75	–
14.3	8.1	–	99.7	–	0.78	–
14.4	11.9	–	108.2	–	0.39	–
15.1	10.1	–	109.4	–	0.59	–
15.2	9.0	–	99.7	–	0.67	–
16.1	6.9	–	69.2	–	0.69	–
16.2	13.6	–	177	–	0.45	–

The impact coefficient C is defined as the ratio between the maximum impact pressure and the product of the density and front velocity square

(with the exception of releases 7.2, 8.1 and 10). In the following we refer to maximum impact pressure values as the peak pressure values measured in the flow front, i.e., before the maximum flow height is attained. In contrast to the flow height time series, no systematic difference is observed between impact pressure time series of first releases or consecutive releases, suggesting that flow height is not a key parameter for determining the impact pressure values. Thus, no correlation between maximum impact pressures and maximum flow heights were assessed. However, the maximum impact pressure values correlate with the square of the front speed (Fig. 10).

The standard deviation values of the raw signal computed over the 0.05-s time interval are proportional to the impact pressure values (see Figs. 9 and 10). They represent 0.23 and 0.39 of the mean pressure values for the large and small pressure plate, respectively. They are low compared to pressure fluctuations measured in dry granular materials that can attain 1 to 10 times the mean pressure values (Albert et al. 1999). In contrast, they are of the same order of magnitude as the fluctuations measured in natural wet snow avalanches composed of polydisperse snow balls (Sovilla et al. 2010). Fluctuations of pressure due to material jamming and

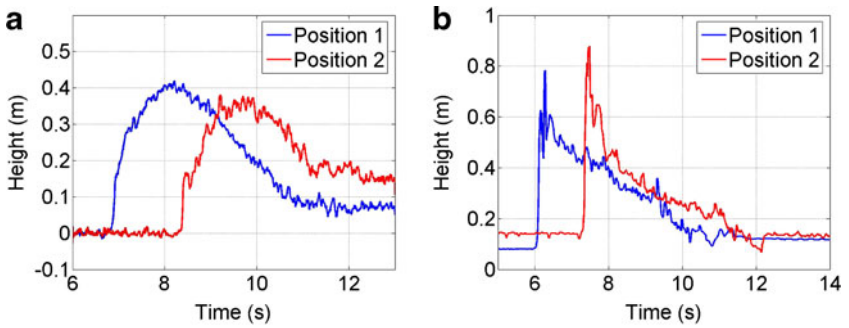

Fig. 6 Flow height versus time at positions 1 and 2 for first release 8.1 (**a**) and second release 14.2 (**b**)

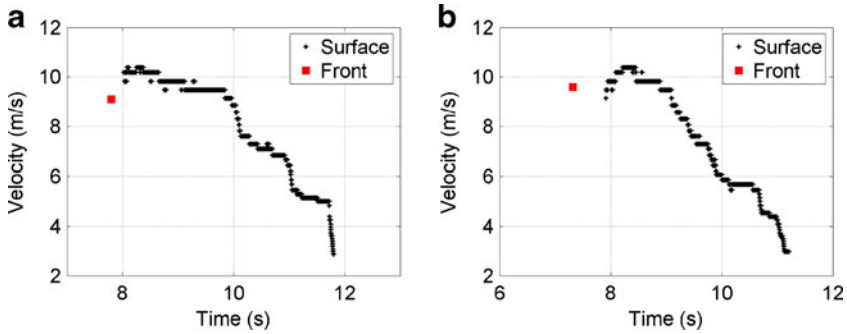

Fig. 7 Flow surface velocity versus time at position 2 and mean flow front velocity for releases 14.1 (**a**) and 14.2 (**b**)

creation/dislocation of force chains between solid grains are thus larger than fluctuations related to hard contacts and to density and velocity inhomogeneities in snow avalanches and hillslope debris flows.

Discussion

With flow heights of the same order of magnitude as the obstacle size, the flow over the entire depth is disturbed at the location of the pressure plates. Material impacting the plates is either deflected around or above the plates or is stopped by the plates (see Fig. 2). In the flow front where the velocities are maximal (see Fig. 7), separation takes place between the flow and the obstacles meaning that the back of the wedges is not in contact with the flow. The relative importance of stopping versus deflection (as well as the direction of deflection) determines the impact pressure.

The main objective of this study is to quantify the impact pressure with respect to the flow parameters including mixture properties, flow height and the flow velocity. Impact pressures exerted by gravitational flows against obstacles have been the subject of many experimental investigations. Two types of empirical formulas are used to describe the impact pressures. Impact height-dependent pressure

$$p = k \cdot \rho \cdot g \cdot H, \tag{3}$$

where ρ is the material density, g is the gravitational acceleration and H is the immersion depth; or velocity-dependent pressure

$$p = C \cdot \rho \cdot u^2, \tag{4}$$

where u is the impact velocity and C is the impact coefficient (e.g., Zanuttigh and Lamberti 2007). The first expression states that the impact pressure is proportional to the static pressure with k as a proportionality coefficient. The second expression relates the impact pressure to the rate of change of momentum of the material. The mass of material encountering the obstacle per unit of time is equal to $A \cdot \rho \cdot u$, where A is the obstacle surface, ρ is the mixture density and u is the impacting velocity. Assuming that the mass is stopped by the obstacle, the force exerted on the obstacle (momentum per unit of time) is given by $A \cdot \rho \cdot u^2$. In reality, not all the material is stopped but part of it is only decelerated or deflected (only if it is all deflected perpendicularly to the plate will the force be the same). Likewise, the flow around the cross section of the obstacle will be altered and thus contribute to the impact pressure. The deviation from the pressure $\rho \cdot u^2$ is accounted for by the impact coefficient C.

Sovilla et al. (2008, 2010) report on impact pressures in snow avalanches. In subcritical flows (Froude number [Fr] <1) (wet snow avalanches and the tails of large dry snow avalanches) the impact pressures are principally height dependant. The proportionality coefficient k is found to be close to 10. For supercritical flows (Fr>1) (dry snow avalanches), impact pressures are reported to depend on velocity and flow density. The computed impact coefficients display a large scatter and are larger than 1. Thibert et al. (2008), in an analysis of one snow avalanche, calculate that the impact coefficient is inversely proportional to the Froude number or equivalently that the impact pressure is proportional to the velocity and to the square root of the flow depth. Impact pressure data from debris flows or landslides are scarce. The Swiss and Hong Kong guidelines for constructing mitigation measures (Egli 2005; GEO Report 2000) recommend the use of the velocity-dependant relationship for the calculation of debris flow impact pressure on obstacles and assign the value of 2 and 3, respectively, to the impact coefficient C.

The dependency on flow height of the impact pressure measured at the Veltheim test site values is found to be negligible: no correlation is apparent between the maximal flow heights and the maximum impact pressure values. The maximum impact pressures, as stated above, represent 2 to 50 times the static pressure derived from the flow heights. Moreover, the impact pressure time series of

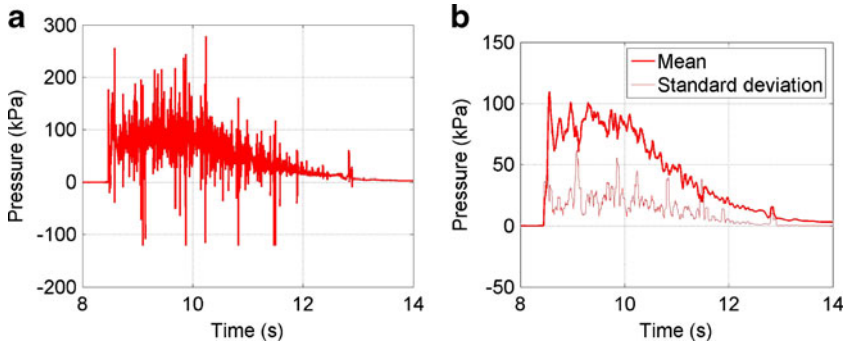

Fig. 8 Impact pressure on the large plate versus time for release 15.1 (**a**) raw signal (**b**) filtered signal with mean value and standard deviation over 0.05-s time intervals. The filter was designed to remove fluctuations arising from the response of the plate to hard contacts

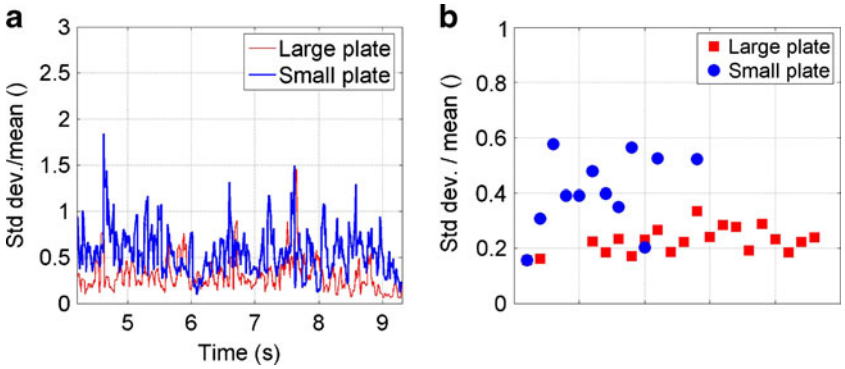

Fig. 9 **a** Ratio time series of standard deviation values of the pressure signal over 0.05-s time interval to mean values of the pressure signal over 0.05-s time interval for release 10 and **b** median values of the ratio time series taken over the duration of the impacts for releases 4 to 16.2

first and consecutive releases are qualitatively similar although the flow height time series are very different. The reason is that the obstacles and flow depths are of the same order of magnitude. Even in the case of consecutive releases with large flow height in the (partially aerated and therefore lower density) front, the overburden pressures at the top of the obstacle are small and thus do not impede deflection of the material.

In the majority of the releases presented above, only the front velocity is available. For the purpose of discussion, we calculate the value of the impact coefficient C based on the front velocity and the "front impact pressure" which is defined as the maximum impact pressure measured during the time when the flow height is increasing. The front velocities between position 2 and 3 range between 2.2 and 13.6 m/s and the front impact pressures between 15 and 200 kPa. The median values of C are 0.64 and 0.90 for the large and small pressure plates respectively (Fig. 9).

For releases 13.1 to 16.2, surface velocity time series are available. They are used together with the impact pressure time series to compute the impact coefficient values over the duration of the impact. One difficulty arises because the surface velocity is computed at position 2 and the impact pressure is measured at position 3. The surface velocity time series are thus extrapolated to position 3 by shifting them in time. The shift in time is chosen as twice the difference between the front passing times at positions 2 and 3 (considering than the front is faster than the rest of the flow). In the first half of the impact duration, the value of the impact coefficient remains nearly constant (Fig. 11), ranging between 0.4 for release 16.1 to 0.8 for releases 13.2 and 15.1. These results are in good agreement with the front impact coefficient values in Fig. 9. In the second half of the impact duration, an increase of the impact coefficient values is observed for some of the releases (in particular 13.1 and 16.2). The reason for this effect may be an artefact of the time shift described above. The extrapolation is accurate in the flow body (where the velocity is about half the front velocity) but it is less precise in the front and in the tail because the time derivative and gradient of the surface velocity in the x-direction are not zero. For practical applications, the first half of the impact corresponds to the time where the velocities are large and in this period of time the impact coefficient values are constant and lower than 1.

Using the velocity-dependent expression, the discrepancies between impact pressures measured by the large and small plates are explained by the different front velocities. The front impact coefficient values are close for the large and small plates, although the scatter is larger for the small plate (the number of measurements by the small plate is smaller, i.e., it partly explains the larger scatter). The difference between the pressures measured by the small and large plates is also related to the fluctuation of the signal. The amplitude of the fluctuations with respect to the mean pressure is twice as large for the small plate (0.39; see Fig. 9b) as for the large plate (0.23). Consequently, the fluctuations are inversely proportional to the size of the obstacle surface, indicating that the length scale of the mass and velocity inhomogeneities are of the same order as the size of the obstacle. For obstacles with surfaces much larger than the scale of the inhomogeneities (i.e., the solid grains), it is expected that the fluctuation dependency on the obstacle size decreases.

In large-scale experiments with similar flows, basal normal stress measurements from 1- and 500-cm^2 sensors are reported by Iverson (1997). Fluctuations of the order of the mean stress were recorded only by the small sensor and are attributed to the granular temperature (i.e., velocity inhomogeneities) of the individual grains, although he describes the possibility of larger scale fluctuations in the presence of clusters of particles. In field measurements in snow avalanches (Sovilla et al. 2010), the fluctuations of the pressure measured by round sensors (0.1 m diameter) are 0.2 to 0.3 of the mean pressure values. However, the source of pressure fluctuations in debris flows and snow avalanches may differ. In debris flows, the

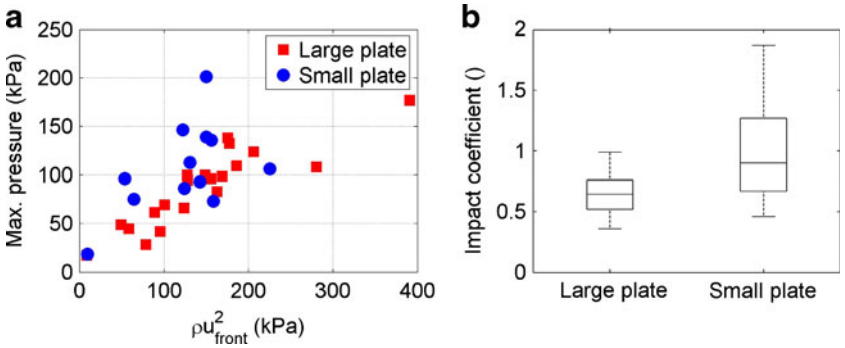

Fig. 10 **a** Maximum impact pressure values versus $\rho \cdot u_{front}^2$ and **b** impact coefficient values for releases 4 to 16.2

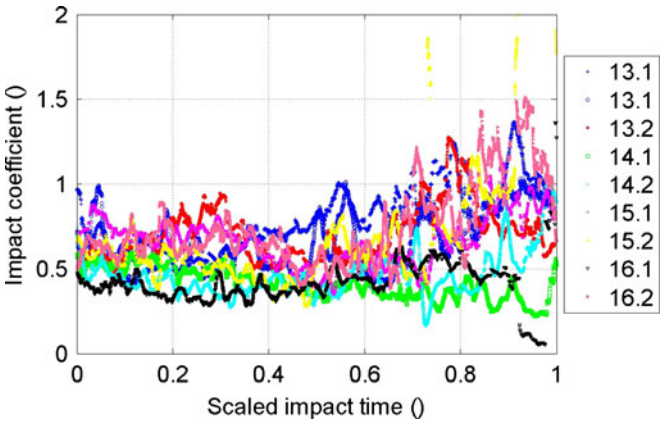

Fig. 11 Impact coefficient values versus scaled impact time for releases 13.1 to 16.2 (with exception of releases 14.3 and 14.4)

fluctuations may arise from density inhomogeneities or from the variable nature of the contacts (from soft to hard, because the muddy interstitial fluid represents a significant portion of the impact mass). In snow avalanches, the fluctuations arising from the velocity fluctuations of the solid snow clumps comprising the granular fluid may dominate, especially at the tail of the avalanche where the density of the flow is constant. Granular effects like material jamming and creation/dislocation of force chains may also contribute to the amplitude of the fluctuations (Sovilla et al. 2010). It is important to recall that in our work the pressure fluctuations, independently from the sensor size, are proportional to the mean pressure values (see Fig. 8b), which themselves scale with the density and with the square of the velocity.

Conclusions and outlook

Calculation guidelines for channelized and hillslope debris flows require reliable estimates of impact pressures on structures and obstacles. In our investigation using field-scale flows, we find that the pressures depend primarily on the flow speed, which in turn appears to depend on the grain-size distribution and water content. The velocities investigated range between 2 and 13 m/s. Thus, the pressure measurements indicate that if the speed can be predicted, for example using a computational model, the impact pressures can be estimated using the quadratic velocity-dependent formula. Impact coefficients C approximately in the range between 0.4 and 0.8 appear to be appropriate for objects with size of the same order of magnitude as the flow heights. Stiff obstacles submerged in mudflows have been reported to have C up to 3; however, we find no experimental verification for such large values.

Clearly, more work is required to investigate alternative flow-obstacle geometries encountered in field problems. The definition of the impact coefficient C should be refined to account for the variability observed at the Veltheim test site. Generally, more quantitative data on flow velocity, flow height and impact pressure are needed to increase the confidence in the prediction of the destructive potential of hillslope debris flows.

Acknowledgements

The authors thank the Swiss Federal Office of the Environment (FOEN) for their financial support of this project "Numerische und experimentelle Grundlagen für die Berechnung von Hangmuren" (numerical and experimental investigations of hillslope debris flows). The authors also thank the technical staff of the WSL Institute for Snow and Avalanche Research (SLF)—most notably Hans Herranhof—for the design and instrumentation of the Veltheim field site. We are grateful to R.M. Iverson for insightful comments on an earlier version of this manuscript.

References

Albert I, Pfeifer MA, Barabàsi AL, Schiffer P (1999) Slow drag in granular medium. Phys Rev Lett 82(1):205–208

Christen M, Kowalski J, Bartelt P (2010) Numerical simulation of avalanches in three-dimensional terrain. Cold Reg Sci Technol 63(1–2):1–14

Egli T (2005) Wegleitung der kantonalen Gebäudeversicherungen—Objektschutz gegen gravitative Naturgefahren

Egli T, Vanomsen P (2005) Schadensanalyse Unwetter 2005—Untersuchung zur Verletzlichkeit von Gebäuden und der Wirksamkeit des Objektschutzes

Geotechnical Engineering Office, The Government of the Hong Kong Special Administrative Region (2000) Review of natural terrain landslide debris-resisting barrier design. GEO Report No. 104

Hutchinson JN (1988) General report: morphological and geotechnical parameters of landslides in relation to geology and hydrogeology. In: Proceedings, Fifth International Symposium on Landslides, vol. 1, pp 3–36

Imura T, Shimojo K (2007) Development und 1:1 field test of impact barrier. Internal note

Iverson RM (1997) The physics of debris flows. Rev Geophys 35(3):245–296

Iverson RM, Logan M, LaHusen RG, Berti M (2010) The perfect debris flow? Aggregated results from 28 large-scale experiments. J Geophys Res 115(F03005):29. doi:10.1029/2009JF001514

Levy A, Sayed M (2008) Numerical simulations of the flow of dilute granular materials around obstacles. Powder Technol 181:137–148

McDougall S, Hungr O (2004) A model for the analysis of rapid landslide motion across three-dimensional terrain. Can Geotech J 41(6):1084–1097

Rickli C, Bücher H (2005) Hangmuren ausgelöst durch die Unwetter vom 15.–16.07.2002 im Napfgebiet und vom 31.08–1.09.2002 im Gebiet Appenzell—Projektbericht zuhanden des Bundesamtes für Wasser und Geologie BWG

Sovilla B, Schaer M, Kern M, Bartelt P (2008) Impact pressures and flow regimes in dense snow avalanches observed at the Vallée de la Sionne test site. J Geophys Res 113:F01010

Sovilla B, Kern M, Schaer M (2010) Slow drag in wet-snow avalanche flow. J Glaciol 56 (198):587–592(6)

Stoffel M, Bollschweiler M (2009) Tree-ring reconstruction of past debris flows based on a small number of samples—possibilities and limitations. Landslides 6(3):225–230

Thibert E et al (2008) Avalanche impact pressure on an instrumented structure. Cold Reg Sci Technol. doi:10.1016/j.coldregions.2008.01.005

Wendeler C (2008) Murgangrückhalt in Wildbächen—Grundlagen zu Planung und Berechnung von flexiblen Barrieren. Dissertation, ETH-Zürich

Zanuttigh B, Lamberti A (2007) Instability and surge development in debris-flows. Rev Geophys 45:RG3006

L. Bugnion (✉) · B. W. McArdell · P. Bartelt
Swiss Federal Institute for Forest, Snow and Landscape Research WSL,
Birmensdorf, Switzerland
e-mail: louis.bugnion@wsl.ch

C. Wendeler
Geobrugg AG,
Romanshorn, Switzerland